SUPPORTING INFORMATION

Beyond a fluorescent probe: Inhibition of cell division protein FtsZ by *mant*-GTP elucidated by NMR and biochemical approaches

Sonia Huecas,[†#] Filipa Marcelo,[†‡#] Almudena Perona,[‖] Laura B. Ruiz-Ávila,[†] Antonio Morreale,[‖] F. Javier Cañada,[†] Jesús Jiménez Barbero,*[†] and José M. Andreu*[†]

[†]Centro de Investigaciones Biológicas, CIB-CSIC, Ramiro de Maeztu 9, 28040 Madrid, Spain

[‡]UCIBIO, REQUIMTE, Dept. de Química, Faculdade de Ciências e Tecnologia, UNL, 2829-516 Caparica, Portugal

[‖]Unidad de Bioinformática, Centro de Biología Molecular, CBMSO-CSIC, Cantoblanco, 28049 Madrid, Spain

CONTENTS: Figures S1 to S6. Molecular dynamics Movies M1_2O′-mant-GTP, M2_3O′-mant-GTP and M3_GTP, which are available free of charge via the Internet at http://pubs.acs.org

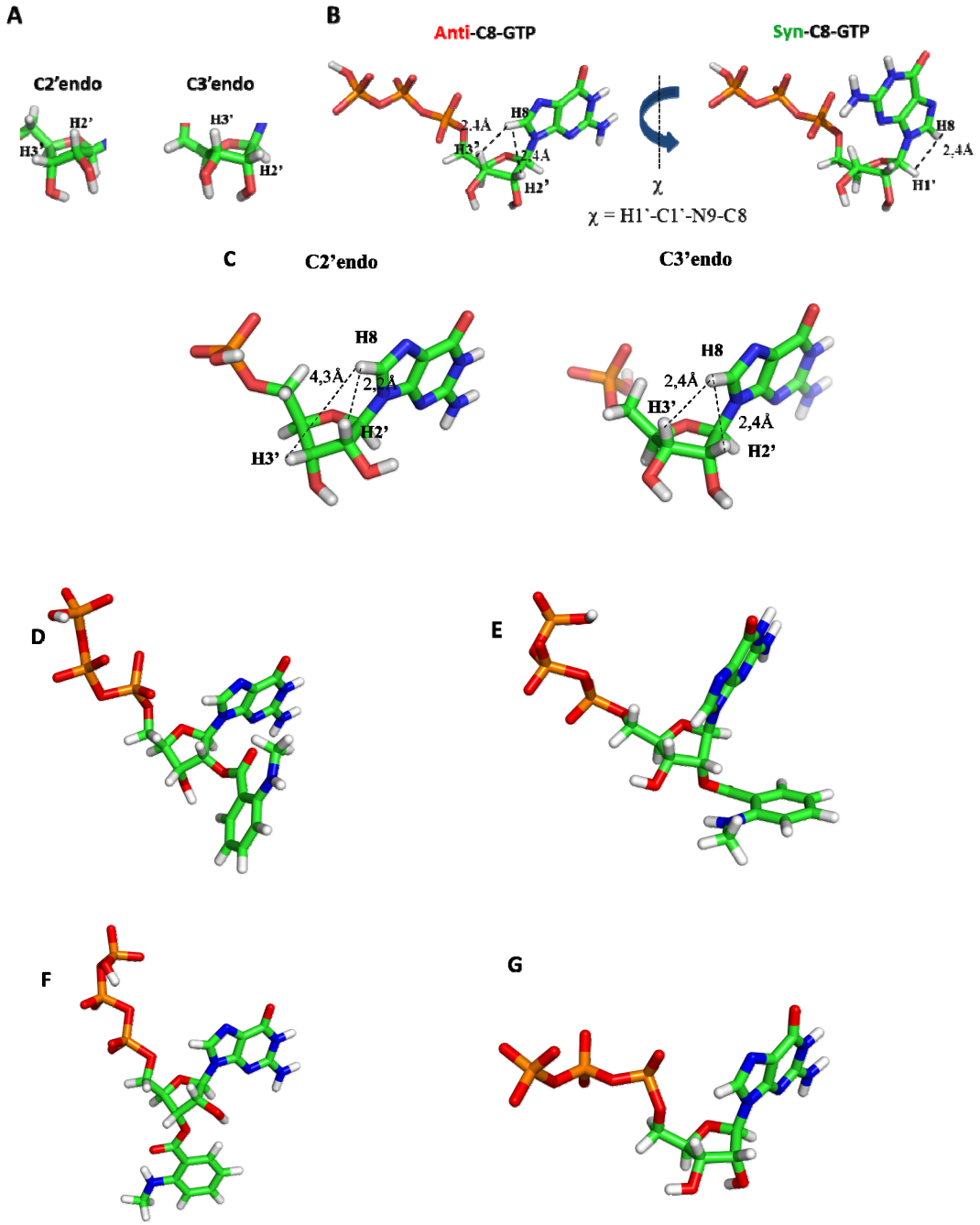

Figure S1, related to Figure 1 and Figure 2A. Guanosine nucleotide conformations. **A.** ribose puckering: C2'endo *vs* C3'endo. **B.** glycosidic torsion angle χ (H1'-C1'-N9-C8) and H/H proton distances for anti or syn-type conformations. **C.** H8-H2' and H8-H3' proton distances for the anti-type conformation and their relation with the C2'endo and C3'endo ribose puckering geometries. **D-F.** Selected mant-GTP structures in agreement with the NMR data that populate the major local minima found by molecular mechanics calculations. **D.** 2'-mant-GTP, anti-type, 2'endo; **E.** 2'-mant-GTP, anti-type, 3'endo; **F.** 3'-mant-GTP, anti-type, 2'endo; **G.** Non substituted GTP, anti-type, 2' endo.

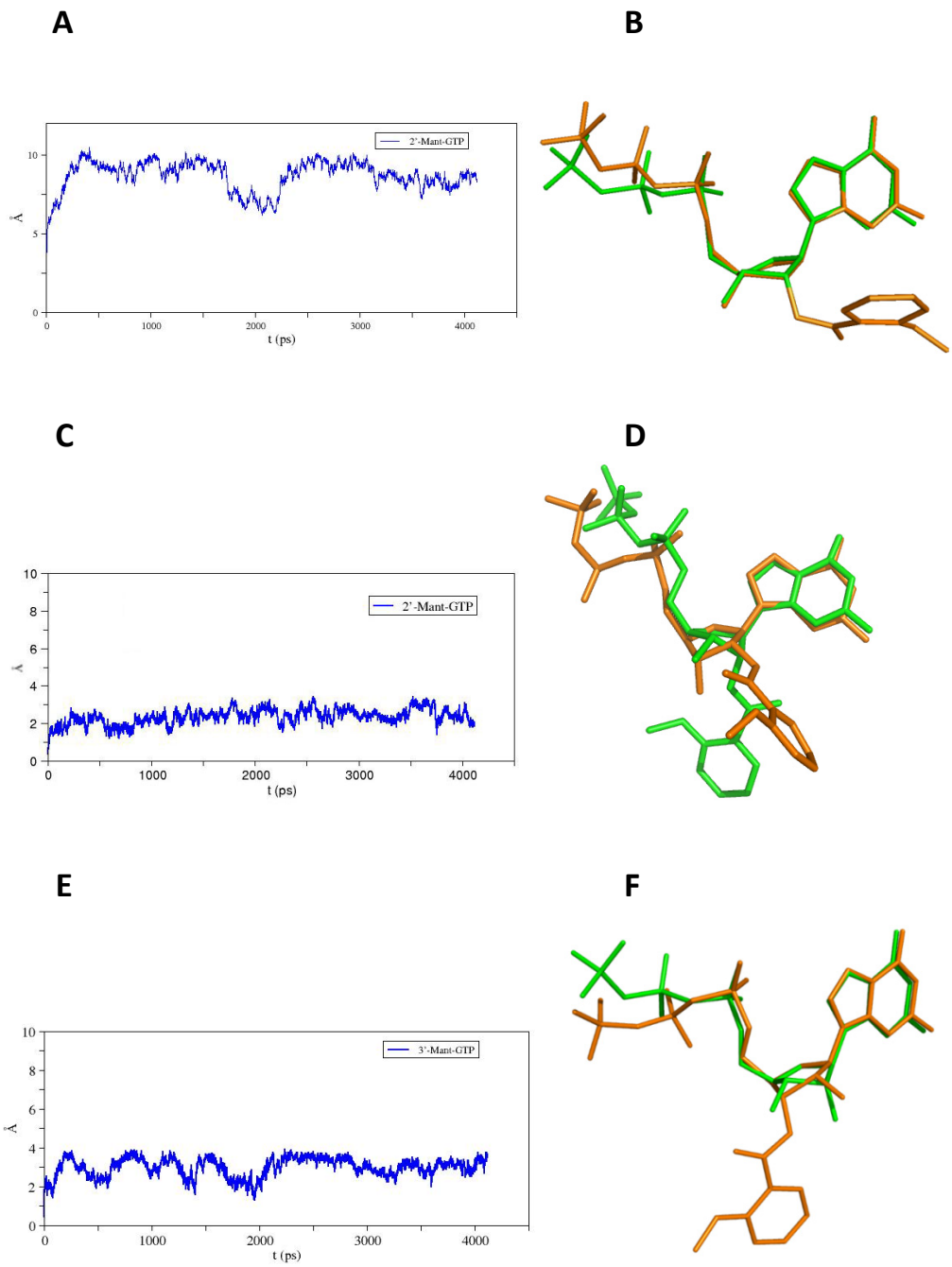

Figure S2. **Molecular dynamics simulations of free mant-GTP, related to main text. A.** RMSD value (Å) evolution along the MD simulation of 2'-mant-GTP C3'-endo in water. 2'-mant-GTP remained in the C3'-endo conformation. **B.** Superposition of the final MD model structure of free 2'-mant-GTP (orange) with the crystal structure of GTP (green) bound to Mj-FtsZ (PDB entry: 1w5a) **C.** RMSD evolution along the MD simulation of 2'-mant-GTP C2' endo, which remained in the C2' endo conformation. **D.** Superposition of the 3'endo (green) and 2'endo (orange) conformations of 2'-mant-GTP. **E**. .RMSD evolution along the MD simulation of 3'-mant-GTP in water. During the first 2 ns, 3'-mant-GTP kept the initial C3'-endo puckering, then it changed to C2'-endo for the remaining time. **F**. Superposition of the final MD model structure of free 3'-mant-GTP (orange, C2'-endo ribose puckering) with the crystal structure of GTP (green, C3'-endo) bound to Mj-FtsZ (PDB: 1w5a).

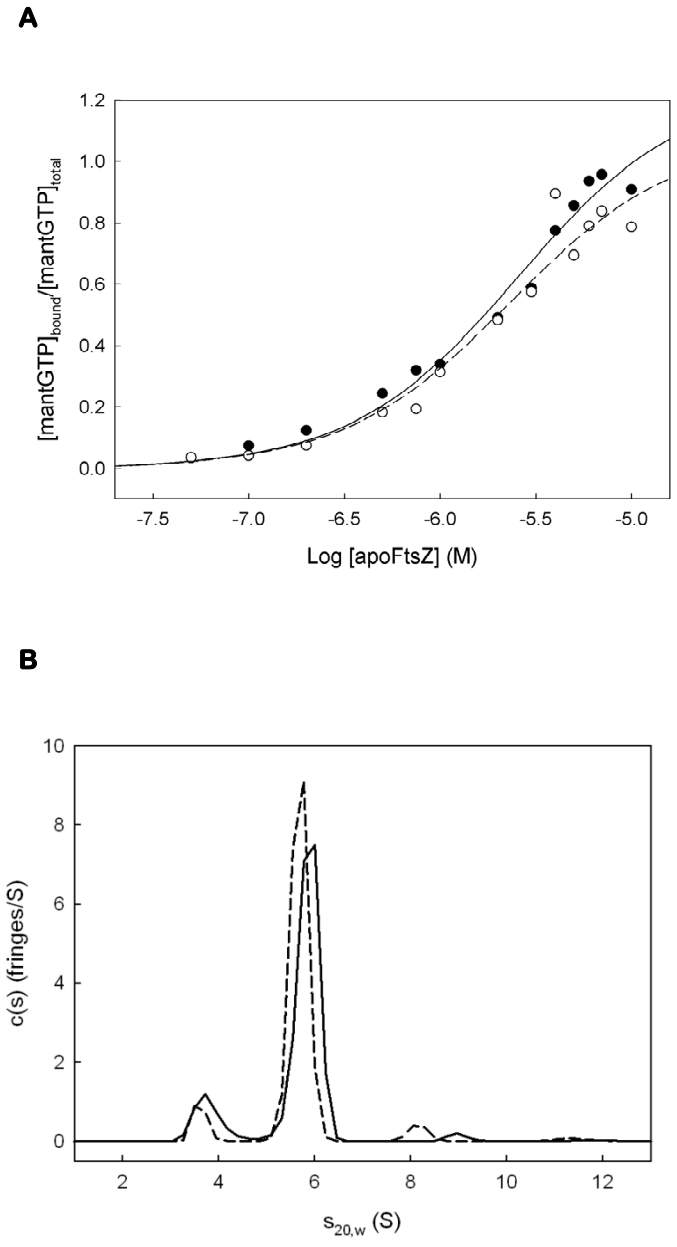

Figure S3, related to Figure 2B-C. **Biochemical characterization of FtsZ-*mant*-GTP interactions under NMR experimental conditions**. **A. Binding of mant-GTP by FtsZ.** Titrations of *mant*-GTP (50 nM) binding by nucleotide-devoid Mj-FtsZ in Tris-H_2O buffer (○) and in D_2O buffer (●), both with 10 mM $MgCl_2$ added, measured by fluorescence anisotropy at 25 °C. The lines in each case correspond to the best single site model fits to the data: K_b (4.3 ± 1.7) x 10^5 M^{-1} in aqueous buffer and (3.9 ± 2.3) x 10^5 M^{-1} in deuterated buffer, with 1.1 ± 0.1 and 1.2 ± 0.1 binding sites respectively**. B. FtsZ association state with *mant*-GTP and GTP.** AUC sedimentation velocity profiles of Mj-FtsZ (30 μM) in Tris-D_2O buffer (no $MgCl_2$) at 25ºC, in the presence of *mant*-GTP (0.6 mM, solid line) or GTP (1.2 mM, dashed line). *Mant*-GTP: 82.2% $s_{20,w}$ =5.8S, 14.5% $s_{20,w}$ =3.8 and 1.9% $s_{20,w}$ =8.9S. GTP: 86.7% $s_{20,w}$ =5.7S, 7.8% $s_{20,w}$ =3.5S and 4% $s_{20,w}$ =8.

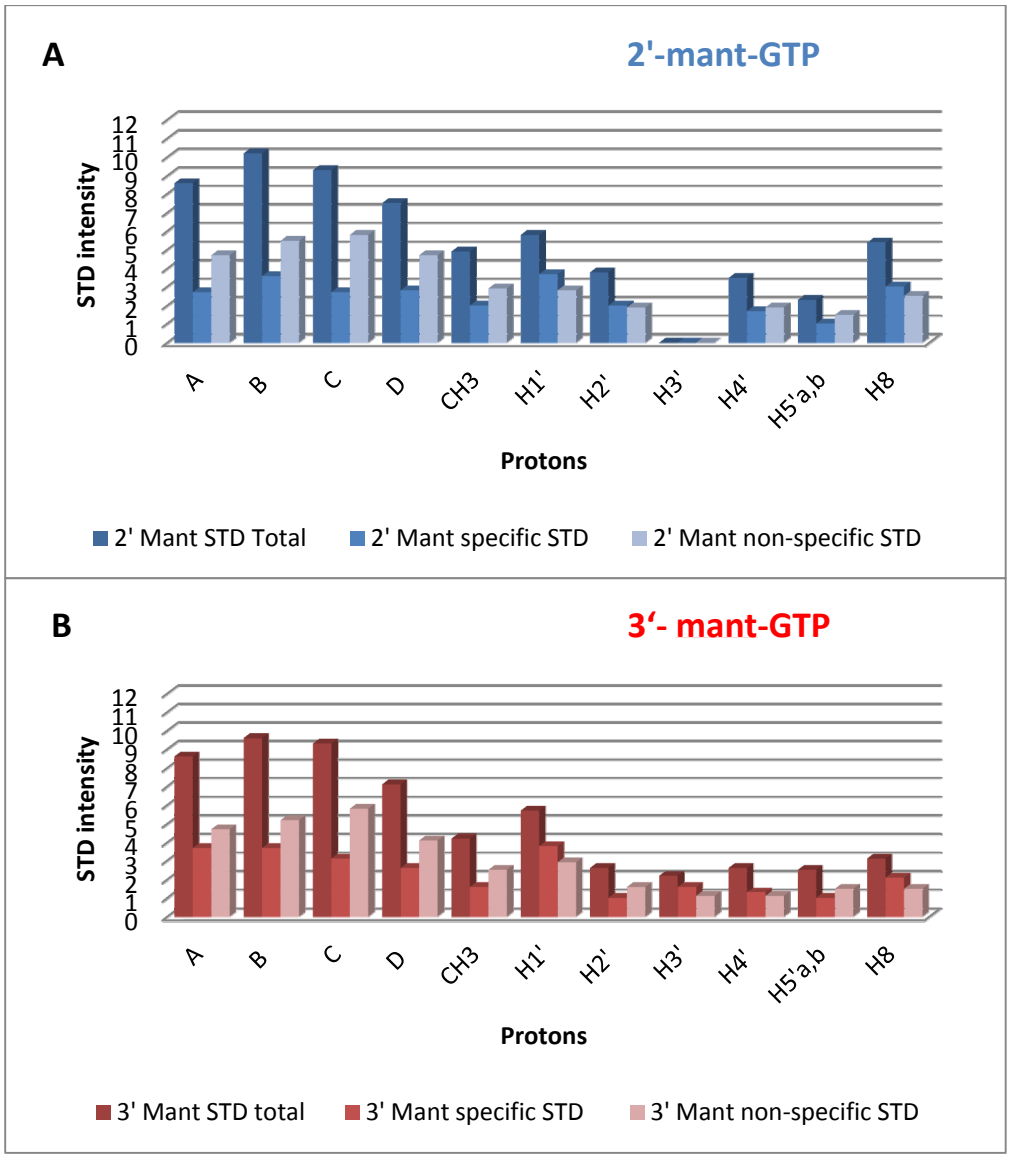

Figure S4, related to Figure 3. STD-NMR total, specific and non-specific intensities in binding experiments of mant-GTP to Mj-FtsZ.. **A.** 2'- mant-GTP **B.** 3'-mant-GTP. Non specific intensities were determined in a 4-fold GTP excess over mant-GTP and subtracted from the total intensities to provide the specific intensities. For both isomers the non-specific contribution mostly arises from the aromatic fluorescent tag moiety. STD intensity values are percentages relative to each off-resonance signal. In the absence of Mj-FtsZ STD intensities were below 0.5% for any of the *mant*-GTP protons measured.

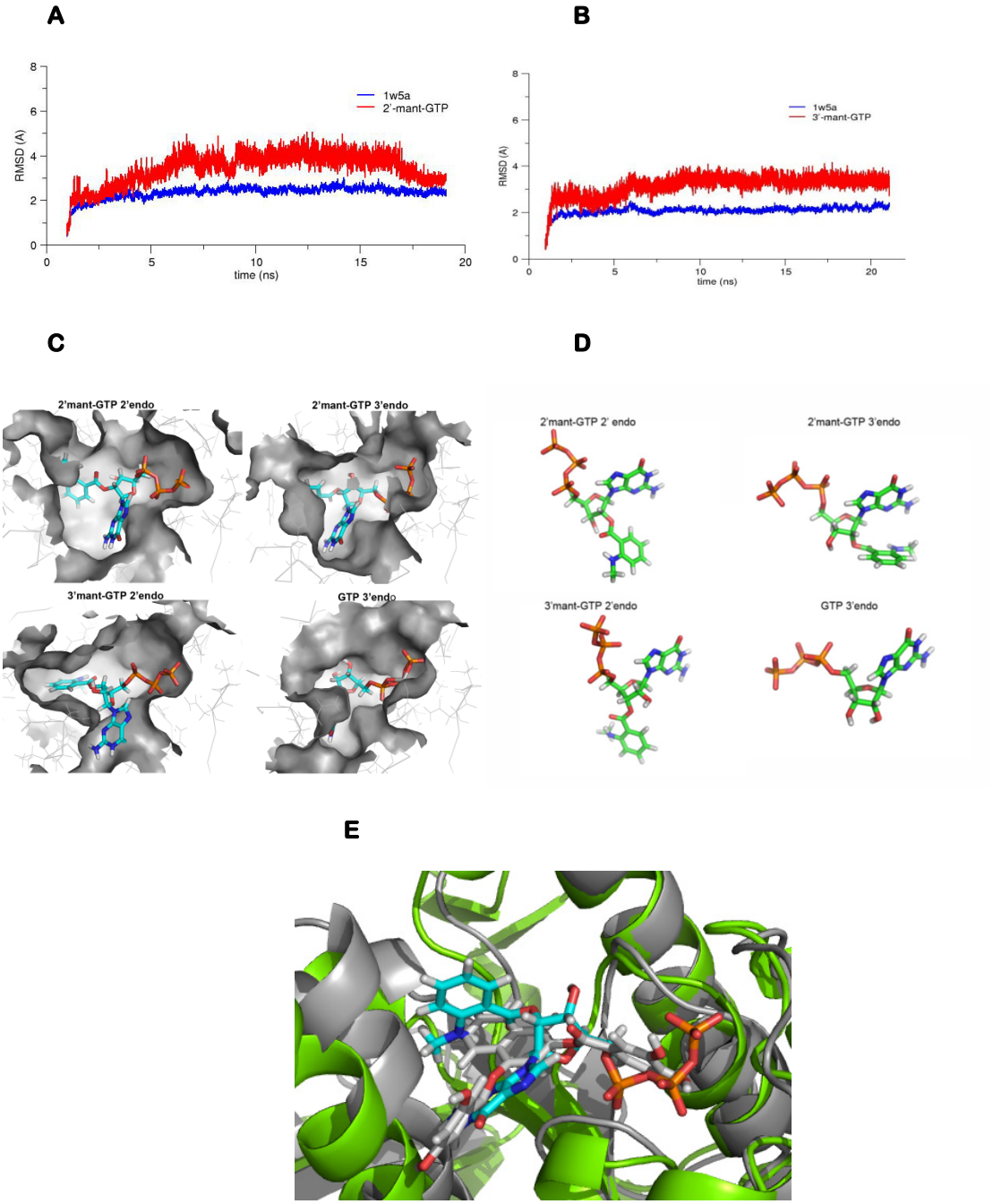

Figure S5, related to Figure 4. **MD simulations of FtsZ-mant-GTP complexes**. **A**. RMSD (Å) evolution along the simulation of the FtsZ-2-'mant-GTP complex. The protein RMSD is depicted in blue and the ligand RMSD is in red. **B.** Corresponding RMSD (Å) values along the simulation of the FtsZ-3'-mant-GTP complex**. C.** 2'-mant-GTP, 3'-mant-GTP, and GTP (atom-colored sticks) bound into the nucleotide binding site of Mj-FtsZ (grey surface representation; from the models in Figure 4). **D.** The different conformations of 2'-mant-GTP, 3'-mant-GTP, and GTP bound to Mj-FtsZ, extracted from the MD models in Figure 4; note that the ligands are colored and presented here in a view similar to the free ligands in Figure S1D-G**. E.** 2'-mant-GTP in the 2'endo conformation bound to a Mj-FtsZ monomer (green protein, cyan ligand; form Figure 4B) aligned to the model complex of Bs-FtsZ with the synthetic inhibitor UCM44 (grey protein and ligand, see main text).

A

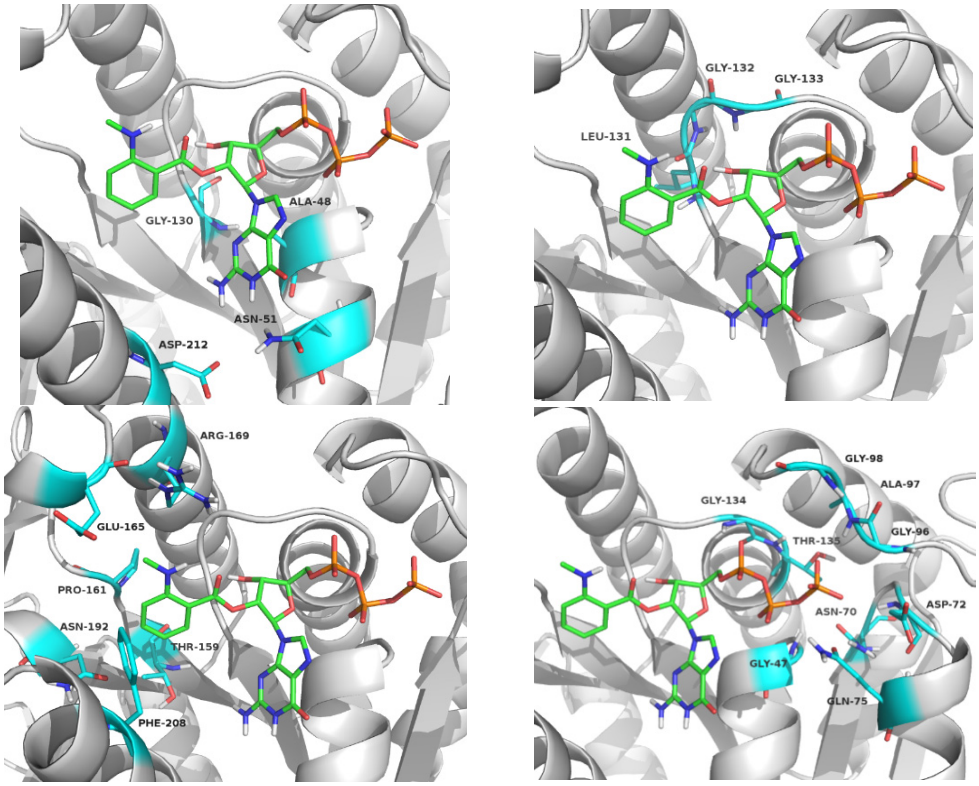
GLY-130
ALA-48
ASN-51
ASP-212
GLY-132
GLY-133
LEU-131
ARG-169
GLU-165
PRO-161
ASN-192
THR-159
PHE-208
GLY-98
ALA-97
GLY-134
GLY-96
THR-135
ASN-70
ASP-72
GLY-47
GLN-75

B

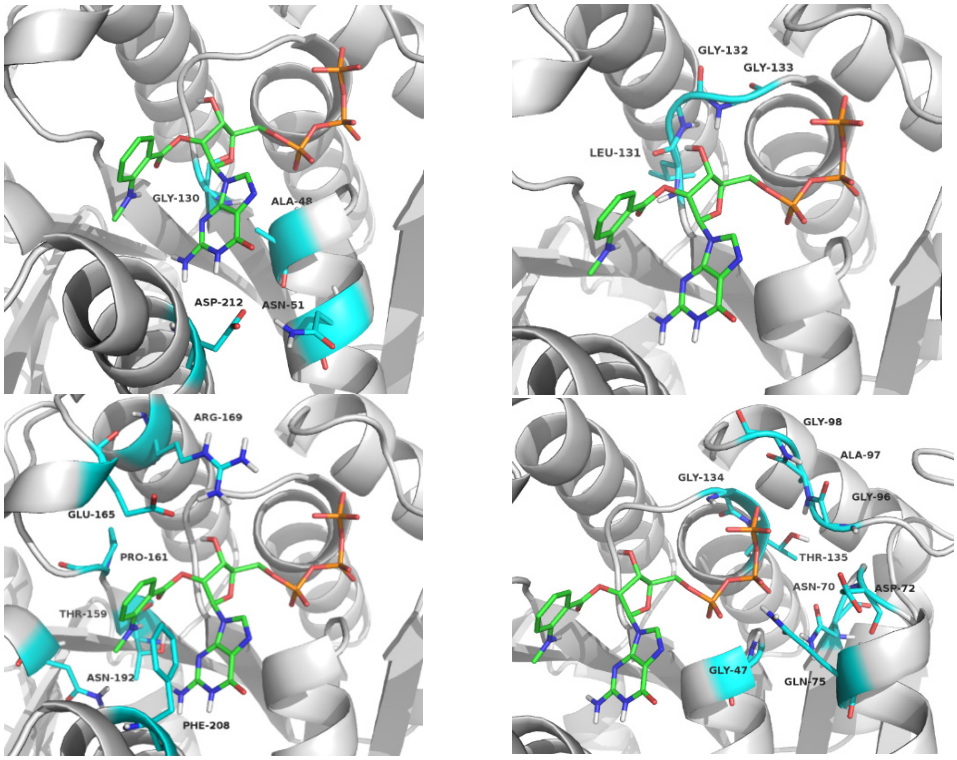
GLY-130
ALA-48
ASP-212
ASN-51
GLY-132
GLY-133
LEU-131
ARG-169
GLU-165
PRO-161
THR-159
ASN-192
PHE-208
GLY-98
ALA-97
GLY-134
GLY-96
THR-135
ASN-70
ASP-72
GLY-47
GLN-75

C

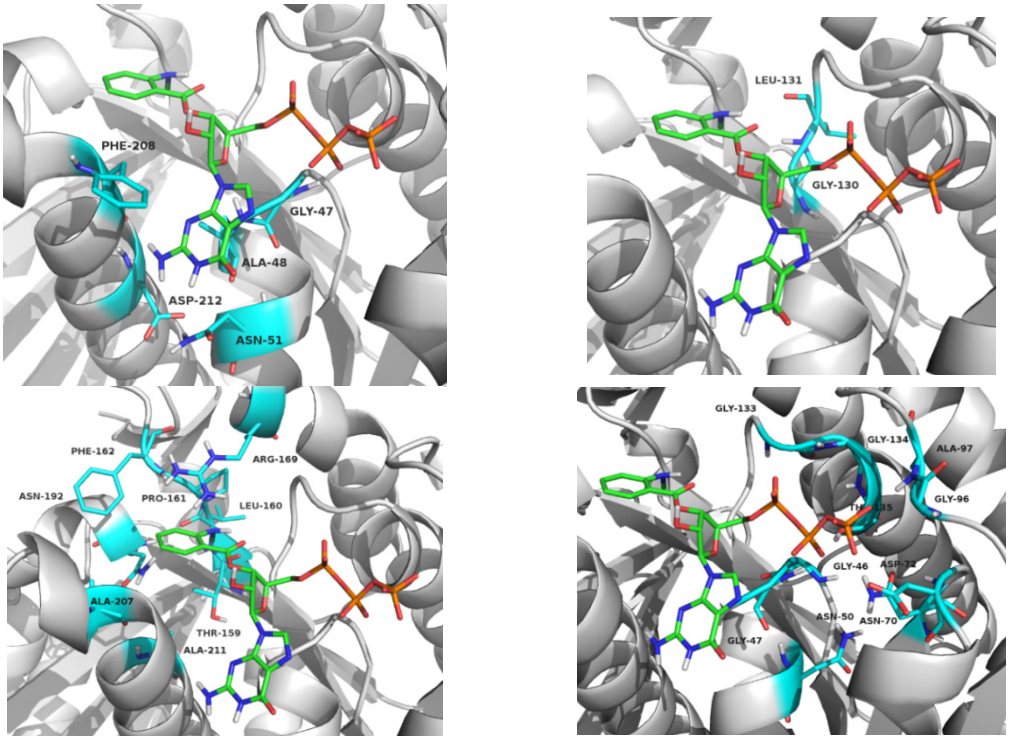

Figure S6, related to Figure 4. A. Aminoacid residues of Mj-FtsZ interacting with 2'-mant-GTP in 2'endo conformation during MD simulations. The main residues contacting the base, phosphates and the *mant* tag are highlighted in blue. **B.** Residues interacting with 2'-mant-GTP in 3'endo conformation. **C.** Residues of Mj-FtsZ interacting with 3'-mant-GTP in 2'endo conformation.

Movies 1, 2 and 3, related to Figure 4, show the molecular dynamics of FtsZ in complex with 2O´-mant-GTP, 3O´-mant-GTP and GTP. They can be found with this supplemental information online